A Pseudo-Label Optimization Method Based on Polar Coordinate Modeling and Prior Constraints

Yudi Wang, Hailan Shen, Yixiao Fu, Yuqi Li, Zeshi Lu, Zailiang Chen*

School of Computer Science and Engineering, Central South University
No. 932, Lushan South Road, Changsha, 410083, Hunan, China

Abstract

Magnetic Resonance Imaging (MRI) and its automatic segmentation are pivotal in assisting physicians with clinical diagnosis. In recent years, with the scarcity of labeled data, significant advancements have been made in semi-supervised segmentation. However, the prediction of many current methods is affected by the presence of false positive regions, which limits their reliability in clinical applications. To tackle this issue, we propose a pseudo-label optimization method based on polar coordinate modeling and prior constraints (PMPC), which refines false positive regions in pseudo-labels by leveraging prior knowledge within the polar coordinate system. Firstly, to improve the efficiency and rationality during polar coordinate modeling, the Adaptive Pole Selection (APS) algorithm is presented to ensure that the pole is located within the foreground region. Secondly, to mitigate false positive regions in pseudo-labels that violate medical anatomical priors, we propose the Prior Knowledge Constraint in Polar Coordinate System (KCP) module to reassign pixel categories in these regions. Finally, the Shape-aware Weighting (SaW) strategy is presented to evaluate the quality of the optimized pseudo-labels based on their shape and then determine their weight in guiding network parameter updates. Experiments on three MRI datasets demonstrate that the proposed method can be effectively integrated with existing pelvic MRI segmentation approaches, significantly reducing false positive rates and further improving segmentation quality.

Code — https://github.com/MAVI-CSU-Lab/PMPC

Introduction

In recent years, the rapid advances in MRI technology and deep learning have led to significant progress in the field of automatic MRI image segmentation using CNN-based networks, aiming to assist clinicians in diagnosis(Shirly and Ramesh 2019). Owing to the difficulties in obtaining medical image datasets and the scarcity of annotated data, semi-supervised learning (SSL) approaches have attracted increasing attention in the field of medical image segmentation(Wang et al. 2022).

Despite the remarkable progress achieved by many existing SSL methods, the presence of false positive regions in the segmentation results remains an unavoidable issue. Such errors can introduce significant interference in practical clinical applications. As illustrated in Figure 1, the masks in Figure 1(a) and (b) enable accurate contour measurement of the target tissues or organs, thereby providing meaningful diagnostic assistance to clinicians. In contrast, when the prediction contains prominent false positive regions, as shown in Figure 1(c), it fails to yield reliable quantitative contour information, rendering it ineffective for clinical use. Similarly, such false positive artifacts are also commonly observed in pseudo-labels during SSL. As training progresses, the model may mistakenly learn incorrect feature representations from these regions and reinforce erroneous predictions, potentially resulting in catastrophic and clinically unreliable segmentation outcomes. To address this problem, recent studies have typically focused on refining pseudo-

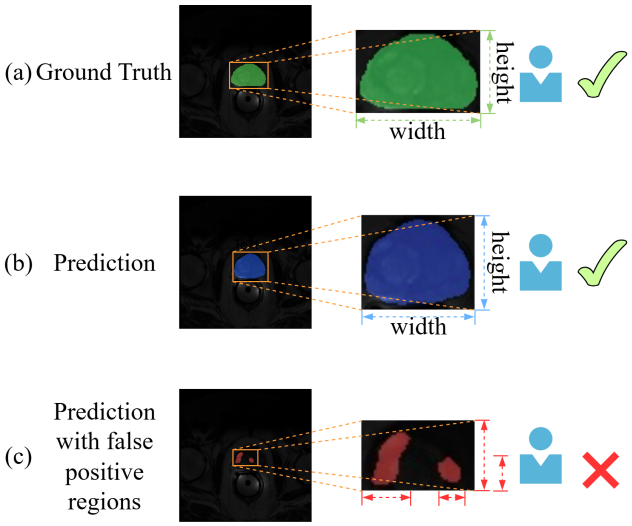

Figure 1: Illustration of how prediction quality affects clinical utility in assisting physicians with measurement and diagnosis. (a) Ground truth labels effectively support accurate measurement and diagnosis. (b) Reasonable predictions can also serve as reliable assistance for clinical evaluation. (c) When false positive regions are present in the prediction, it fails to support measurement and becomes clinically meaningless.

*Corresponding authors.

labels with low accuracy during training in order to enhance their quality. Techniques such as pseudo-label confidence verification(Wang, Peng, and Zhang 2021; Heidari and Guo 2025), consistency regularization(He et al. 2024; Chen et al. 2021), and prior-knowledge-based correction(Gupta et al. 2022) have been proposed. However, these methods are predominantly designed under the Cartesian coordinate system, neglecting certain intrinsic properties of medical images that are more naturally represented in the polar coordinate system. Notably, we observe that the shape priors of many anatomical structures exhibit more regular patterns in polar coordinates—for instance, in many MRI images, the target tissues or organs often demonstrate single connectivity, which is inherently well-suited for modeling in the polar domain.

Motivated by this observation, we propose a pseudo-label optimization method based on polar coordinate modeling and prior constraints (PMPC), aiming to improve the accuracy of pseudo-labels and their alignment with anatomical structures. Specifically, we design the Adaptive Pole Selection (APS) algorithm to improve the rationality of pole placement during polar coordinate modeling. In contrast to existing methods that simply select the pole (Xie et al. 2020, 2021), which may result in the pole being located outside the target region, we determine key pixels from the pseudo-labels based on their confidence scores generated by the pretrained model, and compute the geometric center of the convex hull formed by these pixels as the pole to construct the polar coordinate system. Based on this, we propose the Prior Knowledge Constraint in Polar Coordinate System (KCP) module. By converting the image and pseudo-label contours into their polar representations, we model the inherent anatomical properties of target organs in MRI scans and use them to guide pseudo-label refinement. A Shape-aware Weighting (SaW) strategy is further employed to evaluate the similarity between the refined pseudo-label contours and reference contours, which in turn informs pseudo-label confidence assessment and adaptively weights the loss for model optimization. We validate the proposed method on three MRI datasets, and experimental results demonstrate that our approach outperforms many other state-of-the-art methods in the field of semi-supervised medical image segmentation.

Our main contributions are as follows. (1) We propose a novel method named PMPC, which introduces polar coordinates into pseudo-label optimization for semi-supervised learning for the first time, fully leveraging the inherent advantages of anatomical shape priors in the polar domain. (2) We present the APS algorithm, which explores a rational and effective approach for modeling medical images in polar coordinates. (3) We design the KCP module, which efficiently optimizes pseudo-labels based on medical prior knowledge in the polar coordinate system, thereby improving both the accuracy of pseudo-labels and the performance of semi-supervised learning. (4) We conduct extensive experiments on three MRI datasets, and the results demonstrate that our proposed method outperforms existing state-of-the-art approaches.

Related Work

Pseudo-label Learning in SSL

The core idea of pseudo-label Learning in SSL is to use the model's predictions on unlabeled data as pseudo-labels to guide subsequent training. Mean Teacher(Tarvainen and Valpola 2017) updates the parameters of teacher model based on the student model via an Exponential Moving Average (EMA) strategy. UA-MT(Yu et al. 2019) further incorporates uncertainty information to guide the student network to gradually learn from the high-quality pseudo-labels generated by the teacher network. SLU(Li et al. 2020) optimizes pseudo-labels through iterative self-loop refinement and introduces uncertainty-aware weighting. FixMatch(Sohn et al. 2020) combines consistency regularization with a confidence-based strategy by setting a threshold on the model's prediction confidence, using only high-confidence pseudo-labels for training. PseCo(Li et al. 2022) similarly adopts a high-confidence filtering strategy, combining pseudo-label selection with consistency regularization training to improve the model's generalization ability.

Semi-Supervised Medical Image Segmentation

Currently, many semi-supervised segmentation methods are specifically designed for the medical imaging domain, which build upon general segmentation frameworks and introduce further improvements tailored to medical image segmentation tasks. DHC(Wang and Li 2023) proposes a dual de-biasing heterogeneous co-training framework to dynamically adjust pseudo-labels during training. MCF(Wang et al. 2023) introduces two different sub-networks and leverages the discrepancy between them to correct the model's cognitive bias. EVIL(Chen et al. 2024) leverages uncertainty awareness to propose a more efficient approach for filtering high-confidence pseudo-labels in medical image segmentation. URCA(Qin, Wang, and Zhang 2024) introduces an uncertainty-driven region clipping algorithm that replaces low-confidence pixels with alternative content to create new samples. BCP(Bai et al. 2023) and ABD(Chi et al. 2024) mainly focus on the problem of image distribution alignment under partially labeled data. SGTC(Yan et al. 2025) adopts a semantic-guided training mechanism for consistency learning across three views. Overall, recent studies in this area aim to enhance the quality of pseudo-label generation, thereby facilitating more effective semi-supervised learning.

Method

The overall framework of PMPC is illustrated in Figure 2. PMPC consists of two main stages: a pretraining stage and a pseudo-label optimization stage. In the pretraining stage, PMPC adopts the BSF-Net (Shen et al. 2025) model for initial training, which is conducted for the first half of the total training epochs. In the pseudo-label optimization stage, pseudo-labels are generated using the pretrained model weights. The APS algorithm is applied to select appropriate poles and perform polar coordinate modeling. Subsequently, the KCP module and the SaW strategy are employed to refine the pseudo-labels. The resulting corrected

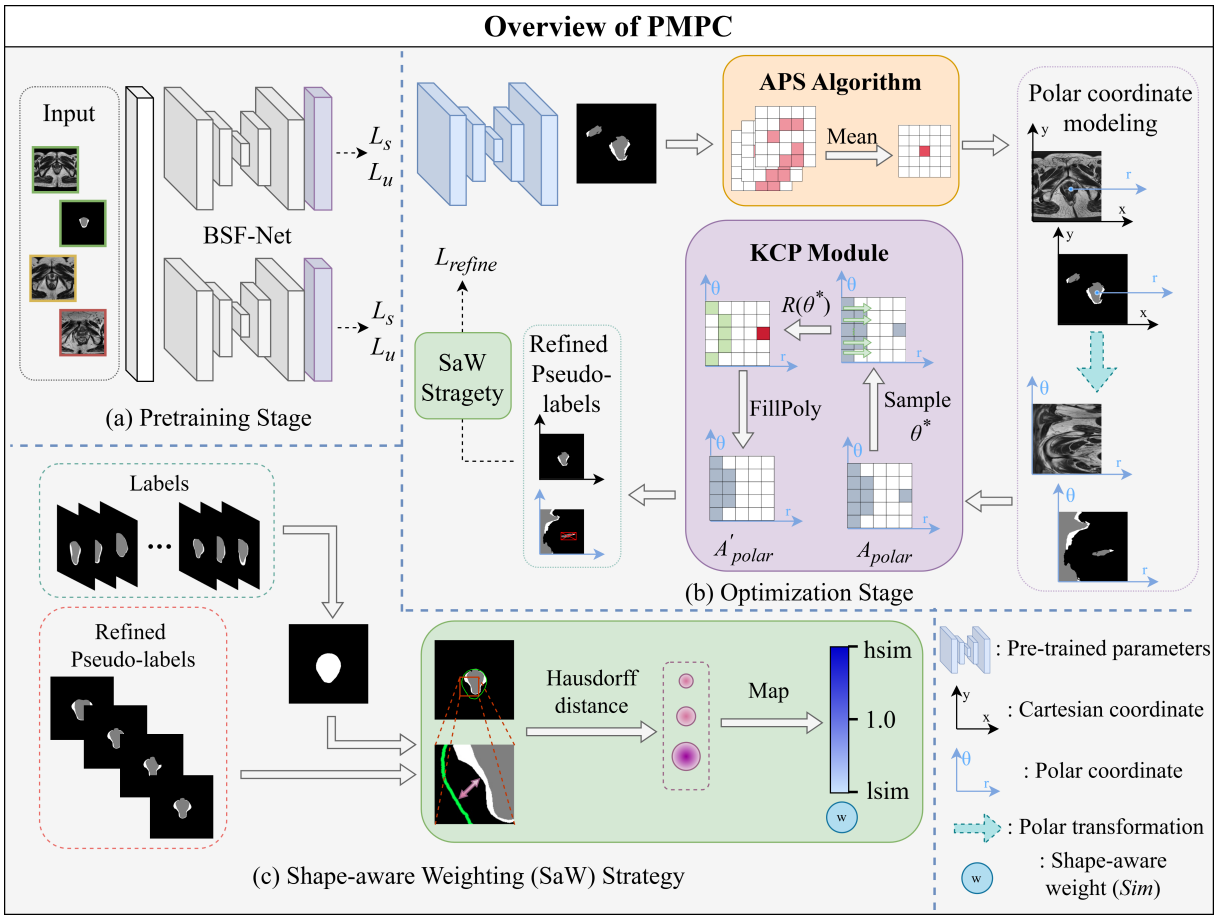

Figure 2: Overview of our PMPC. The overall framework consists of two stages: the pretraining stage (a) and the pseudo-label optimization stage (b). Our proposed Shape-aware Weighting (SaW) strategy is illustrated in (c).

pseudo-labels, along with the newly computed weighted loss, serve as part of the supervision signal for updating the model parameters. The details of each component in PMPC are introduced below.

Adaptive Pole Selection

In MRI image segmentation tasks, many target tissues or organs typically exhibit regional connectivity, with only a single continuous foreground region present in each image. This geometric property is well-suited for representation in the polar coordinate system. To ensure the efficiency of subsequent prior knowledge modeling and reduce computational complexity, it is crucial to select a proper pole during the polar coordinate transformation such that the pole lies within the connected foreground region. The APS algorithm guarantees robust pole localization within the connected foreground region, thereby facilitating more reliable and efficient prior knowledge modeling in the polar domain. The fundamental principle of the APS algorithm is to restrict the pole selection process to a limited subset of high-confidence pixels, rather than incorporating all pixels in the image or the entire foreground region. The comprehensive procedure of the algorithm is delineated in Algorithm 1.

Prior Knowledge Constraint in Polar Coordinate System

In MRI images, many tissues and organs exhibit uniform and continuous structures under normal anatomy. For instance, in our datasets, regions such as the prostate, heart, and pelvic floor muscles consistently present as singular, connected areas. However, pseudo-labels generated in semi-supervised segmentation often lack this singularity and connectivity, frequently containing false positive regions. Incorporating prior knowledge of these structural properties is thus crucial for constraining and refining pseudo-labels during training. This prior knowledge is broadly applicable across various MRI datasets and organs. Given the complexity of assessing connectivity in Cartesian coordinates, we propose the KCP module, which exploits the inherent advantages of the polar coordinate system to effectively model and optimize pseudo-labels. Given a 2D region A representing the foreground area in a pseudo-label, any pixel (x,y) within this region should meet the foreground classification criteria. In Cartesian coordinates, this region is defined as follows:

$$A_{cartesian} = \left\{(x, y) \in R^2 | f\,(x, y) \geq \tau\right\} \quad (1)$$

Algorithm 1: Adaptive Pole Selection

Input: Pretrained network output $\hat{y}$
Output: Pole coordinate list `centroids`

Initialize empty list `centroids`
for each batch in the unlabeled data **do**
  Initialize candidate point set P_c
  $nums\_F \leftarrow$ number of pixels predicted as foreground
  Select foreground pixels (x_i, y_i) with score $> th$ and add to P_c
  $nums\_P \leftarrow$ number of coordinate pairs in P_c
  if $nums\_P < nums\_F \times 1\%$ **then**
    Clear P_c
    Select top $nums\_F \times 1\%$ pixels (x_i, y_i) and add to P_c
  end if
  $(x_{\text{coords}}, y_{\text{coords}}) \leftarrow \text{Mean}(P_c)$
  $\texttt{centroids}.append(x_{\text{coords}}, y_{\text{coords}})$
end for
return `centroids`

Here, $f(x.y)$ denotes a constraint function, and τ represents the threshold used to determine pixel membership within the foreground region. To transform the region from the Cartesian coordinate system to the polar coordinate system, a coordinate transformation is first applied. In the polar coordinate system, a point is represented by its radial distance $r = \sqrt{x^2 + y^2}$ and angle $\theta = \arctan 2(y, x)$. Accordingly, the constraint for region *A* in the polar coordinate system can be formulated as:

$$A_{polar} = \{(r, \theta) \,|g\,(r, \theta) \geq \tau'\} \tag{2}$$

After obtaining the polar coordinate representation of the pseudo-labels, we incorporate anatomical prior knowledge from MRI images into the modeling process within the polar coordinate system. Given that many organ or tissue regions in MRI images manifest as single connected components with relatively regular boundaries and shapes, their contours—when modeled in polar coordinates using a pole located within the connected region—should satisfy the following properties:

$$r\,(\theta) \geq 0, \forall\theta \in [0, 2\pi) \tag{3}$$

$$(r, \theta) \begin{cases} \in A_{polar}, 0 \leq r \leq R\,(\theta) \\ \notin A_{polar}, r \geq R\,(\theta) \end{cases} \tag{4}$$

Here, $r(\theta)$ denotes the contour curve representing the boundary of the foreground region, and (r, θ) represents a pixel coordinate pair in the polar coordinate system. $R(\theta)$ associated with a given θ indicates the radial distance from the pole to the boundary of the foreground region at that angle. The objective is to determine $R(\theta)$ to delineate a reasonable foreground region within the pseudo-label. Given that MRI images typically have a resolution of 256 × 256 pixels, the foreground contour $r(\theta)$ is inherently discrete rather than a perfectly continuous curve. To ensure computational tractability, we uniformly sample n discrete angles over the interval $[0, 2\pi)$, and compute the corresponding radial distances $R(\theta)$ as follows:

Algorithm 2: Uniform Sampling-Based Computation of $R(\theta)$

Input: Set of selected angles θ^*, boundary width r_0
Output: Set of radius values $R(\theta)^*$

Initialize empty list $R(\theta)^*$
for each θ_i in θ^* **do**
  $flag \leftarrow$ False ▷ Signal for entering foreground region
  while $r \leq r_{\max}$ **do**
    if $g(r, \theta_i) \geq \tau'$ **and** not $flag$ **then**
      $flag \leftarrow$ True ▷ First enter foreground
    else if $g(r, \theta_i) < \tau'$ **and** $g(r + r_0, \theta_i) < \tau'$ **and** $flag$ **then**
      $R(\theta_i) \leftarrow r + r_0$
      break
    end if
  end while
end for
return $R(\theta)^* = \{R(\theta_i) \mid i = 0, 1, 2, \ldots, n-1\}$

$$\theta^* = \left\{\theta_i | \theta_i = \frac{2\pi i}{n}, i = 0, 1, 2, ..., n-1\right\} \tag{5}$$

The corresponding $R(\theta)^*$ are calculated based on the uniformly sampled set θ^*, as described in Algorithm 2. Using $R(\theta)^*$ obtained from Algorithm 2, multiple boundary pixels are connected to form a closed contour that approximates the foreground region constraint in the pseudo-labels. Pixels located outside this enclosed contour are considered false positives, and the pseudo-labels are subsequently refined. This process can be formally expressed as follows:

$$A'_{polar} = \left\{(r, \theta) \,|g'\,(r, \theta) = \text{FillPoly}\left(R\,(\theta)^*, 1\right)\right\} \tag{6}$$

$$A'_{cartesian} = \left\{(x, y) \in R^2 | f'\,(x, y) = 1\right\} \tag{7}$$

$$\hat{y}_{refine} = \hat{y} \otimes A'_{cartesian} \tag{8}$$

Here, A'_{polar} and $A'_{cartesian}$ are initialized to zero. The function FillPoly denotes a rasterization algorithm used for region filling, which fills the closed area enclosed by the pixels in θ^* with 1. $\otimes$ denotes element-wise multiplication and $\hat{y}_{refine}$denotes the pseudo-labels optimized under prior knowledge constraints.

Shape-aware Weighting

After applying prior knowledge constraints, the original pseudo-label theoretically removes false positive regions and retains only the unique foreground connected region. When supervising the network's predictions using these optimized pseudo-labels, it is still necessary to consider their confidence to further reduce the information bias introduced

during model training. Therefore, we proposes SaW strategy. By calculating the shape similarity between the optimized pseudo-label and the prior knowledge contour, the confidence of the pseudo-label is assessed, and then mapped to a certain range to assign appropriate weights to the loss function, thereby assisting model training.

Initially, the average foreground contour is derived from the ground truth labels across the entire labeled dataset, serving as the shape constraint during the shape-aware procedure, as described as follows:

$$h\left(x,y\right)=\frac{1}{N_L}\sum_{i=1}^{N_L}y_i \tag{9}$$

$$Y_{shape}=\begin{cases}1, h\left(x,y\right)>0\\ 0, h\left(x,y\right)=0\end{cases} \tag{10}$$

Subsequently, the Hausdorff distance is used to quantify the discrepancy between the shape constraint and the optimized pseudo-label, thus assessing the pseudo-label's confidence. The computed Hausdorff distance is then mapped to a specified interval $[lsim, hsim]$ to serve as the shape-aware weight, which is incorporated into the loss calculation of the optimization method described in this chapter, as shown as follows:

$$Sim=\max\left(lsim, hsim-H\left(Y_{shape},\hat{y}_{refine}\right)/max\_hd\right) \tag{11}$$

Here, $lsim<1<hsim$, max_hd is the preset maximum distance, set to 400 in this work, and Sim denotes the computed shape-aware weight. Finally, the loss function of our proposed PMPC optimization method is expressed as:

$$L_{refine}=Sim\cdot\sum\nolimits_{i=1}^{N_U}y_{refine}^{i}\cdot\log(\hat{y}^{i}) \tag{12}$$

and the overall loss function used throughout the training process is defined as:

$$L=L_s+\alpha\cdot L_u+\beta\cdot L_{refine} \tag{13}$$

Specifically, L_s denotes the supervised loss, which is a combination of Dice loss and cross-entropy loss, while L_u represents the unsupervised loss, for which cross-entropy loss is employed.

Experiments

Dataset

PROMISE12 (Litjens et al. 2014) is a benchmark for prostate MRI segmentation. Following the common practice in recent SOTA methods, we utilize data from 50 patients in total and they are split into training, validation, and test sets in a ratio of 7:1:2. We conduct experiments under two labeled data settings, utilizing 10% and 20% of the training samples as labeled data.

ACDC (Bernard et al. 2018) is a widely used benchmark dataset for cardiac MRI segmentation. Following other researches, we utilize 100 patients in total and adopt the same data partitioning as PROMISE12. We conduct experiments under 5% and 10% labeled data in training set.

The Female Pelvic dataset is a pelvic MRI dataset consisting of 221 T2-weighted MRI scans from 96 patients. We split the dataset into training, validation, and test sets with a ratio of 7:1:2. Furthermore, we set two different proportions of labeled data for training: 10% and 20%.

Implementation Details

All experiments are conducted on an NVIDIA GeForce GTX 1080Ti. We use the U-net (Ronneberger, Fischer, and Brox 2015) architecture as our backbone network and adopt BSF-Net as the pretrained network. α is kept consistent with that used in SSL4MIS (Luo 2020), and β is set to 1. n is set to 36, r_0 is set to 5, and $lsim$ and $hsim$ are set to 0.8 and 1.2, respectively. th is set to 0.999 for the PROMISE12 and Female Pelvic datasets and 0.9 for the ACDC dataset. The batch size is set to 8 for the PROMISE12 and ACDC datasets and 2 for the Female Pelvic dataset. The learning rate is initialized to 0.01 for the ACDC and Female Pelvic datasets and to 0.05 for the PROMISE12 dataset. We use the SGD optimizer with a decaying learning rate throughout the training process and adhere to the weight decay strategy and other settings followed SSL4MIS. To minimize the impact of randomness, each experiment is conducted in triplicate. The final results are presented as the mean values and the corresponding standard deviations of the three experiments on four evaluation metrics: Dice Score (Dice), Jaccard Score (Jaccard), 95% Hausdorff Distance (95HD), and Average Surface Distance (ASD).

Comparison with SOTA Methods

The effectiveness of the proposed method is validated through experimentation on the above three datasets, with comparisons made against current SOTA semi-supervised medical image segmentation methods, including Unet (Ronneberger, Fischer, and Brox 2015), MT (Tarvainen and Valpola 2017), CPS (Chen et al. 2021), SSNet (Wu et al. 2022), SCP-Net (Zhang et al. 2023), Cross-ALD (Nguyen-Duc et al. 2023), DCNet (Chen et al. 2023), BCP (Bai et al. 2023), UniMatch (Yang et al. 2023), CorrMatch (Sun et al. 2024), SAMT-PCL (Chen, Chen, and Huang 2024) and ABD(Chi et al. 2024).

Comparison Results on PROMISE12 Dataset: Table 1 presents the experimental results on the PROMISE12 dataset. As shown in Table 1, our proposed method achieves the best performance across all evaluation metrics and shows a significant improvement compared to existing state-of-the-art (SOTA) methods. For example, under the 20% labeled setting, our proposed PMPC method outperforms ABD by 3.74% in terms of the Dice score. Figure 3 further provides a visual comparison of the segmentation results from different methods on the PROMISE12 dataset. It is evident from the figure that the predictions generated by PMPC are the closest to the ground truth, with significantly fewer false positive regions than other methods.

Comparison Results on ACDC Dataset: Table 2 presents the experimental results on the ACDC dataset. Our PMPC method also achieves outstanding segmentation performance, attaining the best results in most comparison ex-

Method	10% Labeled Data				20% Labeled Data			
	Dice↑	Jaccard↑	95HD↓	ASD↓	Dice↑	Jaccard↑	95HD↓	ASD↓
Unet(MICCAI, 2015)	42.74±2.43	4.03±2.35	15.46±0.93	5.23±0.51	57.41±3.52	48.12±3.41	14.90±1.54	6.41±0.78
MT(NeurIPS, 2017)	55.79	45.70	23.65	10.92	59.21±3.73	50.25±3.28	16.49±2.19	7.27±1.40
CPS(CVPR, 2021)	60.43±1.61	49.93±1.51	23.13±4.49	11.05±2.31	71.89±3.02	61.54±2.68	11.86±1.88	4.59±0.54
SSNet(MICCAI, 2022)	60.78±1.36	51.27±1.10	15.12±1.38	5.94±1.10	70.09±2.44	59.69±1.64	13.04±1.42	3.60±0.55
SCP-Net*(MICCAI, 2023)	66.21	/	/	11.56	77.06	/	/	3.52
DCNet*(MICCAI, 2023)	68.89	54.88	12.93	3.75	78.68	65.44	10.65	2.53
BCP(CVPR, 2023)	69.28±1.15	59.49±1.75	8.39±1.89	2.29±0.68	75.65±1.72	65.10±1.34	9.99±1.34	2.93±0.38
UniMatch(CVPR, 2023)	74.26±0.91	62.89±1.05	13.55±1.50	4.66±0.91	77.54±1.04	66.57±1.11	6.56±0.82	1.46±0.39
Corrmatch(CVPR, 2024)	75.56±0.94	65.01±1.00	11.35±1.57	4.27±0.74	79.13±3.28	68.41±4.04	12.94±0.74	4.36±0.29
SAMT-PCL*(ESA, 2024)	70.93	57.03	9.40	3.08	78.45	65.35	6.28	1.81
ABD*(CVPR, 2024)	81.81	/	/	1.46	82.06	/	/	1.33
PMPC(Ours)	**83.17±2.24**	**74.97±2.06**	**3.52±0.05**	**0.63±0.04**	**85.80±1.07**	**77.74±0.93**	**3.23±0.18**	**0.68±0.08**

Table 1: Comparison with state-of-the-art semi-supervised segmentation methods on the PROMISE12 dataset. We report the mean±std (standard deviation) of the three replicated experiments. Evaluation results marked with * are taken from the original papers. Results for other methods are obtained from our replication using their original codes.

Method	5% Labeled Data				10% Labeled Data			
	Dice↑	Jaccard↑	95HD↓	ASD↓	Dice↑	Jaccard↑	95HD↓	ASD↓
Unet(MICCAI, 2015)	48.85±1.92	38.38±1.85	27.99±5.23	11.50±2.05	81.15±0.72	69.91±1.09	9.20±0.47	2.69±0.12
MT(NeurIPS, 2017)	64.54±2.89	52.90±2.48	23.02±2.20	7.68±0.60	85.32±0.72	75.49±0.84	10.99±1.45	3.06±0.60
CPS(CVPR, 2021)	72.48±1.84	62.38±2.36	6.84±1.21	1.64±0.56	87.55±0.46	78.64±0.67	6.61±0.19	2.07±0.20
SSNet*(MICCAI, 2022)	65.82	55.38	6.67	2.28	86.78	77.67	6.07	1.40
SCP-Net*(MICCAI, 2023)	71.14	/	/	4.65	87.27	/	/	2.65
Cross-ALD*(MICCAI, 2023)	80.60	69.08	5.96	1.90	87.52	78.62	4.81	1.60
DCNet*(MICCAI, 2023)	70.36	60.78	3.94	0.86	89.42	81.37	**1.28**	**0.38**
BCP*(CVPR, 2023)	87.59	78.67	1.90	0.67	88.84	80.62	3.98	1.17
UniMatch(CVPR, 2023)	74.89±1.30	62.79±1.30	11.92±0.34	3.40±0.08	84.64±0.42	74.30±0.58	10.80±3.27	2.88±0.54
Corrmatch(CVPR, 2024)	85.70±1.23	75.81±1.72	4.47±0.58	1.38±0.18	87.48±0.09	78.47±0.12	4.93±0.58	1.46±0.11
SAMT-PCL*(ESA, 2024)	74.39	63.94	5.07	1.42	88.62	80.11	2.06	0.60
ABD*(CVPR, 2024)	88.96	80.70	**1.57**	0.52	89.81	81.95	1.46	0.49
PMPC(Ours)	**89.01±0.34**	**80.72±0.54**	1.63±0.14	**0.48±0.02**	**90.10±0.17**	**82.48±0.25**	1.49±0.19	0.46±0.04

Table 2: Comparison with state-of-the-art semi-supervised segmentation methods on the ACDC dataset.

Method	10% Labeled Data				20% Labeled Data			
	Dice↑	Jaccard↑	95HD↓	ASD↓	Dice↑	Jaccard↑	95HD↓	ASD↓
Unet(MICCAI, 2015)	73.57±2.12	61.55±2.51	12.71±0.55	3.19±0.19	77.68±2.87	66.16±3.74	5.55±0.34	1.53±0.04
MT(NeurIPS, 2017)	76.25±1.43	64.37±1.87	8.71±0.60	1.88±0.20	79.37±1.80	68.60±2.81	4.83±0.76	1.23±0.24
CPS(CVPR, 2021)	79.06±0.70	68.13±1.03	4.52±0.50	1.13±0.16	81.59±0.61	71.29±0.93	4.58±0.59	1.13±0.14
SSNet(MICCAI, 2022)	77.92±1.03	66.45±1.26	5.57±1.10	1.35±0.34	80.09±0.93	69.34±1.19	5.16±0.35	1.26±0.15
DCNet(MICCAI, 2023)	80.64±1.60	70.22±1.90	3.34±0.38	0.63±0.06	81.11±2.04	71.29±2.61	4.22±0.62	0.83±0.15
BCP(CVPR, 2023)	74.93±0.90	63.43±1.01	4.57±0.23	0.79±0.07	79.22±0.55	68.42±0.78	3.40±0.20	0.66±0.06
UniMatch(CVPR, 2023)	76.70±0.53	65.18±0.57	6.18±0.17	1.30±0.08	80.63±0.21	70.13±0.24	3.09±0.14	0.80±0.08
Corrmatch(CVPR, 2024)	79.07±1.15	68.08±1.43	4.51±0.54	1.22±0.15	80.98±0.49	70.71±0.62	4.07±0.40	0.99±0.14
ABD(CVPR, 2024)	81.45±0.08	70.98±0.18	5.68±1.63	1.25±0.20	82.35±0.31	72.17±0.44	5.57±0.31	1.29±0.05
PMPC(Ours)	**83.11±0.03**	**73.27±0.04**	**2.55±0.02**	**0.60±0.01**	**83.16±0.08**	**73.39±0.10**	**2.65±0.21**	**0.65±0.06**

Table 3: Comparison with state-of-the-art semi-supervised segmentation methods on the Female Pelvic dataset.

periments. Under the 10% labeled setting, our method ranks second only in 95HD and ASD, likely due to the irregular shapes in ACDC where DCNet's boundary refinement offers an edge. Moreover, the comparison uses the best results

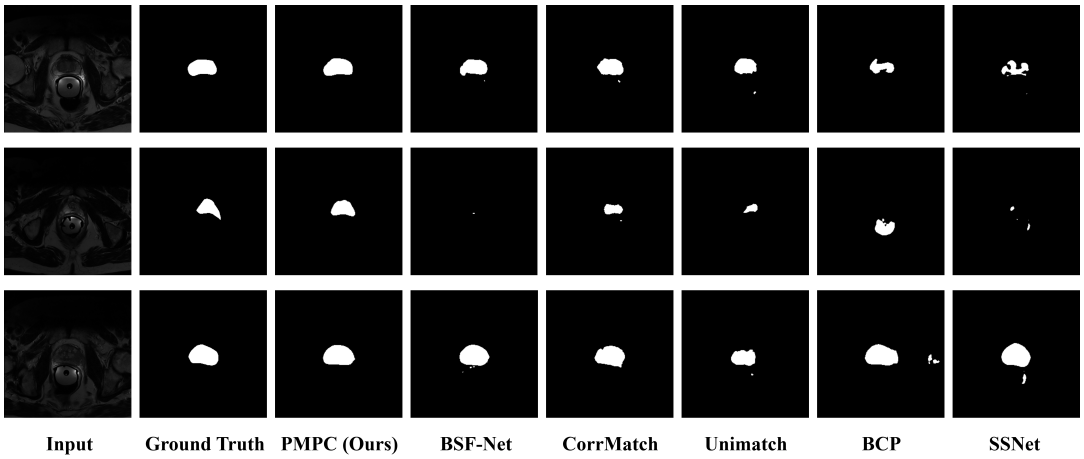

Figure 3: Visualization of comparative methods on the PROMISE12 dataset under 10% labeled data.

baseline	KCP	SaW	Dice↑	Jaccard↑	95HD↓	ASD↓
✓			81.11	72.23	5.47	1.65
✓	✓		85.13	77.10	3.52	**0.67**
✓	✓	✓	**85.80**	**77.74**	**3.23**	0.68

Table 4: Ablation studies on the PROMISE12 dataset with 20% labeled data, validating the effectiveness and compatibility of the proposed KCP and SaW respectively.

from prior work, while ours are averaged over three runs, which may also contribute to the slight performance gap.

Comparison Results on the Female Pelvic Dataset: Table 3 presents the comparison results on the private dataset against state-of-the-art methods. We can find that our PMPC outperforms existing methods in all metrics, which further demonstrates its effectiveness and superiority.

Ablation Studies

We conduct a series of ablation experiments to verify the impact of each component in the proposed method, as well as the effects of different cutting strategies and hyperparameter settings.

Ablation study of each component: Table 4 presents the ablation study results of the KCP modules and SaW strategy in the PMPC framework, conducted on the PROMISE12 dataset with 20% labeled data. We can find that KCP yields a 4.02% improvement in Dice score, and SaW further enhances performance by 0.67%, demonstrating the effectiveness and compatibility of the two modules.

Ablation study of pole selection strategies: Table 5 presents the impact of different pole selection strategies on the experimental results, based on the PROMISE12 dataset with 10% labeled data. We compared two pole selection methods: using the image center and using the geometric center of the foreground region. In contrast, the proposed APS outperforms both by addressing their limitations, demonstrating its critical role in improving the quality of polar coordinate modeling.

Pole Selection Strategies	Dice↑	Jaccard↑	95HD↓	ASD↓
image center	77.29	69.16	4.94	0.91
foreground center	78.85	70.64	5.33	1.30
APS	**83.17**	**74.97**	**3.52**	**0.63**

Table 5: Ablation study under different pole selection strategies on the PROMISE12 Dataset with 10% labeled data.

n	Dice↑	Jaccard↑	95HD↓	ASD↓
12	81.86	71.54	3.33	0.79
36	83.11	73.27	2.55	0.60
108	83.13	73.30	2.53	0.60

Table 6: Ablation studies under different setting of sampling density n on the Female Pelvic Dataset with 10% labeled data.

Ablation study of sampling density n: In addition, we analyze the impact of the sampling density of θ, denoted as n, which is shown in Table 6 based on the private dataset with 10% labeled data. Considering the balance between label smoothness and computational efficiency, we set n to 36 in our experiments.

Conclusion

In this paper, we propose a novel pseudo-label optimization method based on polar coordinate modeling and prior constraints (PMPC) to address the issue of false positives in semi-supervised medical image segmentation. A new adaptive pole selection algorithm is designed to enhance the quality of polar coordinate modeling. Furthermore, prior anatomical knowledge is incorporated in the polar coordinate space to constrain and refine pseudo-labels, fully leveraging the advantages of this representation. In addition, we perform real-time quality assessment of the optimized pseudo-labels to ensure their reliability during training. Extensive experiments on three MRI datasets demonstrate the effectiveness of the proposed PMPC, with evaluation metrics significantly outperforming existing SOTA methods.

Acknowledgements

This manuscript was supported in part by the Natural Science Foundation of Hunan Province under Grant 2025JJ50369, the Changsha Municipal Natural Science Foundation under Grant kq2502090. The authors wish to acknowledge High Performance Computing Center of Central South University for computational resources.

References

Bai, Y.; Chen, D.; Li, Q.; Shen, W.; and Wang, Y. 2023. Bidirectional copy-paste for semi-supervised medical image segmentation. In *Proceedings of the IEEE/CVF conference on computer vision and pattern recognition*, 11514–11524.

Bernard, O.; Lalande, A.; Zotti, C.; Cervenansky, F.; Yang, X.; Heng, P.-A.; Cetin, I.; Lekadir, K.; Camara, O.; and Ballester, M. A. G. 2018. Deep learning techniques for automatic MRI cardiac multi-structures segmentation and diagnosis: is the problem solved? *IEEE transactions on medical imaging*, 37(11): 2514–2525.

Chen, F.; Fei, J.; Chen, Y.; and Huang, C. 2023. Decoupled Consistency for Semi-supervised Medical Image Segmentation. In *International Conference on Medical Image Computing and Computer-Assisted Intervention*, 551–561. Springer.

Chen, X.; Yuan, Y.; Zeng, G.; and Wang, J. 2021. Semi-supervised semantic segmentation with cross pseudo supervision. In *Proceedings of the IEEE/CVF conference on computer vision and pattern recognition*, 2613–2622.

Chen, Y.; Chen, F.; and Huang, C. 2024. Combining contrastive learning and shape awareness for semi-supervised medical image segmentation. *Expert Systems with Applications*, 242: 122567.

Chen, Y.; Yang, Z.; Shen, C.; Wang, Z.; Zhang, Z.; Qin, Y.; Wei, X.; Lu, J.; Liu, Y.; and Zhang, Y. 2024. Evidence-based uncertainty-aware semi-supervised medical image segmentation. *Computers in Biology and Medicine*, 170: 108004.

Chi, H.; Pang, J.; Zhang, B.; and Liu, W. 2024. Adaptive bidirectional displacement for semi-supervised medical image segmentation. In *Proceedings of the IEEE/CVF conference on computer vision and pattern recognition*, 4070–4080.

Gupta, S.; Hu, X.; Kaan, J.; Jin, M.; Mpoy, M.; Chung, K.; Singh, G.; Saltz, M.; Kurc, T.; Saltz, J.; et al. 2022. Learning topological interactions for multi-class medical image segmentation. In *European Conference on Computer Vision*, 701–718. Springer.

He, A.; Li, T.; Wu, Y.; Zou, K.; and Fu, H. 2024. FRCNet: Frequency and Region Consistency for Semi-supervised Medical Image Segmentation. In *International Conference on Medical Image Computing and Computer-Assisted Intervention*, 305–315. Springer.

Heidari, M.; and Guo, Y. 2025. Bi-Level Optimization for Semi-Supervised Learning with Pseudo-Labeling. In *Proceedings of the AAAI Conference on Artificial Intelligence*, 17168–17176.

Li, G.; Li, X.; Wang, Y.; Wu, Y.; Liang, D.; and Zhang, S. 2022. Pseco: Pseudo labeling and consistency training for semi-supervised object detection. In *European Conference on Computer Vision*, 457–472. Springer.

Li, Y.; Chen, J.; Xie, X.; Ma, K.; and Zheng, Y. 2020. Self-loop uncertainty: A novel pseudo-label for semi-supervised medical image segmentation. In *Medical Image Computing and Computer Assisted Intervention–MICCAI 2020: 23rd International Conference, Lima, Peru, October 4–8, 2020, Proceedings, Part I 23*, 614–623. Springer.

Litjens, G.; Toth, R.; Van De Ven, W.; Hoeks, C.; Kerkstra, S.; Van Ginneken, B.; Vincent, G.; Guillard, G.; Birbeck, N.; and Zhang, J. 2014. Evaluation of prostate segmentation algorithms for MRI: the PROMISE12 challenge. *Medical image analysis*, 18(2): 359–373.

Luo, X. 2020. SSL4MIS. https://github.com/HiLab-git/SSL4MIS.

Nguyen-Duc, T.; Le, T.; Bammer, R.; Zhao, H.; Cai, J.; and Phung, D. 2023. Cross-adversarial local distribution regularization for semi-supervised medical image segmentation. In *International Conference on Medical Image Computing and Computer-Assisted Intervention*, 183–194. Springer.

Qin, C.; Wang, Y.; and Zhang, J. 2024. URCA: Uncertainty-based region clipping algorithm for semi-supervised medical image segmentation. *Computer Methods and Programs in Biomedicine*, 254: 108278.

Ronneberger, O.; Fischer, P.; and Brox, T. 2015. U-net: Convolutional networks for biomedical image segmentation. In *Medical image computing and computer-assisted intervention–MICCAI 2015: 18th international conference, Munich, Germany, October 5-9, 2015, proceedings, part III 18*, 234–241. Springer. ISBN 3319245732.

Shen, H.; Wang, Y.; Chen, Z.; Xiong, W.; Wu, W.; and Liu, H. 2025. BSF-Net: Balancing small foreground regions for semi-supervised segmentation of MRI. *Optics & Laser Technology*, 112422.

Shirly, S.; and Ramesh, K. 2019. Review on 2D and 3D MRI image segmentation techniques. *Current Medical Imaging*, 15(2): 150–160.

Sohn, K.; Berthelot, D.; Carlini, N.; Zhang, Z.; Zhang, H.; Raffel, C. A.; Cubuk, E. D.; Kurakin, A.; and Li, C.-L. 2020. Fixmatch: Simplifying semi-supervised learning with consistency and confidence. *Advances in neural information processing systems*, 33: 596–608.

Sun, B.; Yang, Y.; Zhang, L.; Cheng, M.-M.; and Hou, Q. 2024. Corrmatch: Label propagation via correlation matching for semi-supervised semantic segmentation. In *Proceedings of the IEEE/CVF Conference on Computer Vision and Pattern Recognition*, 3097–3107.

Tarvainen, A.; and Valpola, H. 2017. Mean teachers are better role models: Weight-averaged consistency targets improve semi-supervised deep learning results. *Advances in neural information processing systems*, 30.

Wang, H.; and Li, X. 2023. Dhc: Dual-debiased heterogeneous co-training framework for class-imbalanced semi-supervised medical image segmentation. In *International*

conference on medical image computing and computer-assisted intervention, 582–591. Springer.

Wang, R.; Lei, T.; Cui, R.; Zhang, B.; Meng, H.; and Nandi, A. K. 2022. Medical image segmentation using deep learning: A survey. *IET Image Processing*, 16(5): 1243–1267.

Wang, Y.; Peng, J.; and Zhang, Z. 2021. Uncertainty-aware pseudo label refinery for domain adaptive semantic segmentation. In *Proceedings of the IEEE/CVF international conference on computer vision*, 9092–9101.

Wang, Y.; Xiao, B.; Bi, X.; Li, W.; and Gao, X. 2023. Mcf: Mutual correction framework for semi-supervised medical image segmentation. In *Proceedings of the IEEE/CVF conference on computer vision and pattern recognition*, 15651–15660.

Wu, Y.; Wu, Z.; Wu, Q.; Ge, Z.; and Cai, J. 2022. Exploring smoothness and class-separation for semi-supervised medical image segmentation. In *International conference on medical image computing and computer-assisted intervention*, 34–43. Springer.

Xie, E.; Sun, P.; Song, X.; Wang, W.; Liu, X.; Liang, D.; Shen, C.; and Luo, P. 2020. Polarmask: Single shot instance segmentation with polar representation. In *Proceedings of the IEEE/CVF conference on computer vision and pattern recognition*, 12193–12202.

Xie, E.; Wang, W.; Ding, M.; Zhang, R.; and Luo, P. 2021. Polarmask++: Enhanced polar representation for single-shot instance segmentation and beyond. *IEEE Transactions on Pattern Analysis and Machine Intelligence*, 44(9): 5385–5400.

Yan, K.; Cai, Q.; Zhang, F.; Cao, Z.; and Liu, Z. 2025. SGTC: semantic-guided triplet Co-training for sparsely annotated semi-supervised medical image segmentation. In *Proceedings of the AAAI Conference on Artificial Intelligence*, 9112–9120.

Yang, L.; Qi, L.; Feng, L.; Zhang, W.; and Shi, Y. 2023. Revisiting weak-to-strong consistency in semi-supervised semantic segmentation. In *Proceedings of the IEEE/CVF Conference on Computer Vision and Pattern Recognition*, 7236–7246.

Yu, L.; Wang, S.; Li, X.; Fu, C.-W.; and Heng, P.-A. 2019. Uncertainty-aware self-ensembling model for semi-supervised 3D left atrium segmentation. In *Medical image computing and computer assisted intervention–MICCAI 2019: 22nd international conference, Shenzhen, China, October 13–17, 2019, proceedings, part II 22*, 605–613. Springer.

Zhang, Z.; Ran, R.; Tian, C.; Zhou, H.; Li, X.; Yang, F.; and Jiao, Z. 2023. Self-aware and cross-sample prototypical learning for semi-supervised medical image segmentation. In *International Conference on Medical Image Computing and Computer-Assisted Intervention*, 192–201. Springer.